AGRICULTURAL AND FOREST METEOROLOGY 149 (2009) 230–243

available at www.sciencedirect.com

ScienceDirect

journal homepage: www.elsevier.com/locate/agrformet

Evapotranspiration and energy balance of native wet montane cloud forest in Hawai'i

Thomas W. Giambelluca [a,*], Roberta E. Martin [a,b], Gregory P. Asner [b], Maoyi Huang [c,b], Ryan G. Mudd [a], Michael A. Nullet [a], John K. DeLay [a], David Foote [d]

[a] Department of Geography, University of Hawai'i at Mānoa, Honolulu, HI 96822, United States
[b] Department of Global Ecology, Carnegie Institution, Stanford, CA 94305, United States
[c] Department of Civil, Structural, and Environmental Engineering, The State University of New York, Buffalo, NY 14260, United States
[d] Pacific Islands Ecosystems Research Center, Klauea Field Station, Hawai'i National Park, HI 96718, United States

ARTICLE INFO

Article history:
Received 21 March 2008
Received in revised form
12 August 2008
Accepted 12 August 2008

Keywords:
Tropical montane cloud forests
Evapotranspiration
Energy balance
Throughfall
Forest hydrology
Hawai'i Volcanoes National Park

ABSTRACT

Evapotranspiration (ET) and energy balance were observed, using eddy covariance and other micrometeorological measurements, at a native *Metrosideros polymorpha* forest site in Hawai'i. Total rainfall for the 12-month study period (2401 mm) was close to the long-term mean (2500 mm year^{-1}), but was highly variable from month to month with distinct dry periods in February, May, and December 2005. Measured annual ET of 996 mm year^{-1} was slightly higher than previous estimates for similar locations in Hawai'i. However, the energy closure ratio was 0.784, leading us to adjust turbulent energy fluxes upward by 27.6%. The resulting adjusted annual ET of 1232 mm is significantly higher than previous forest ET estimates for Hawai'i. Variations in canopy conductivity suggest that midday stomatal closure is occurring and/or that evaporation is high in the morning because of frequent wet canopy conditions early in the day. The daily fraction of turbulent energy flux used for ET was observed to be lower for days with high net radiation, indicating that transpiration is being limited under conditions of high evaporative demand. ET was generally higher during rainy periods than dry periods. After controlling for differences in available energy, ET is, on average, 29% higher on days with rain than days without rain. The fraction of energy used for ET follows a distinct annual pattern, roughly corresponding to the observed cycle in leaf area at the site, with a minimum in mid-April and a maximum in mid-October. Variations in rainfall appear to be the cause of deviations from the annual cycle of the fraction of energy used for ET. This suggests that ET is strongly controlled by variations in canopy wetness at this wet forest site.

© 2008 Elsevier B.V. All rights reserved.

1. Introduction

Tropical montane forests with frequent fog are zones of great hydrological and ecological value. Within the cloud zone, vegetation strips droplets from the passing air, thereby increasing water input. Because of cloud water interception and persistent rainfall, tropical montane cloud forests (TMCFs) generate high watershed yields, supporting water resource needs of downstream regions. Ecologically, TMCFs often form "islands" of biodiversity, supporting a high proportion of endemic species (Merlin and Juvik, 1993; Bruijnzeel and Hamilton, 2000). Loss of forest cover in these zones greatly reduces fog interception, potentially altering the regional hydrology. Effects of global climate change (Still et al., 1999;

* Corresponding author.
E-mail address: thomas@hawaii.edu (T.W. Giambelluca).
0168-1923/$ – see front matter © 2008 Elsevier B.V. All rights reserved.
doi:10.1016/j.agrformet.2008.08.004

Pounds et al., 1999) and regional land cover change (Lawton et al., 2001) threaten to elevate the cloud base and reduce or eliminate many existing TMCFs.

Field studies (Hutley et al., 1997; Waterloo et al., 1999; Schellekens et al., 2000) have shown that tropical maritime forests sustain exceptionally high rates of evapotranspiration (ET). Observations have shown evaporation of rainfall intercepted by vegetation (E_i) to be very high at sites in Indonesia (Bruijnzeel and Wiersum, 1987), Brunei (Dykes, 1997), and Puerto Rico (Scatena, 1990; Schellekens et al., 2000), and transpiration (E_t) to be very high at a drier leeward site on Viti Levu, Fiji (Waterloo et al., 1999). These findings support Shuttleworth (1989) observations of high ET in coastal and island forests and place a high priority on improving ET estimates in other maritime tropical forests. In Hawai'i, wet montane forest areas are critically important sources of groundwater recharge and host threatened ecological resources. Planning for water development and protection of fragile ecosystems in Hawai'i depend on accurate quantification of hydrological processes in forests. However, no prior stand-level measurements of ET have ever been made in Hawaiian forests.

The partitioning of energy by forests is a dominant control on climate and hydrology at local to global scales. Recent studies in similar maritime tropical environments suggest that forest ET in Hawai'i may exceed current estimates by significant amounts (e.g. Waterloo et al., 1999). Accurate forest ET measurements in Hawai'i are urgently needed to test the reproducibility of exceptionally high rates found elsewhere, and to answer specific questions about hydrological processes in Hawai'i. In this study, we employ intensive field measurements to quantify evapotranspiration and energy balance in a native forest in Hawai'i's wet windward cloud zone.

2. Background

In high rainfall areas of Hawai'i's forested slopes, ET is seldom moisture limited, and hence potential evapotranspiration (PE) methods, including the Penman equation and evaporimeter measurements, have been used as estimates of ET. PE estimates by Mink (1962), Takasaki et al. (1969) and Ekern (1983), all showed an inverse relationship between ET and rainfall in very wet areas, with annual ET of approximately 500 mm for locations receiving 5000 mm annual rainfall (RF). To date, ET has been assumed to be limited by low net radiation and high humidity in persistently cloudy, humid mountain slopes within or beneath the orographic cloud zone. All subsequent water budgets for Hawai'i's important groundwater recharge areas have been based on these assumptions. For example, these assumptions have been used in root-zone water balance models to estimate ET and recharge on O'ahu (Giambelluca, 1983, 1986; Giambelluca et al., 1996), Kaua'i (Shade, 1995a), Moloka'i (Shade, 1997) and the North Kohala region of Hawai'i Island (Shade, 1995b; Oki, 2002). The resulting ET estimates increase with increasing RF up to a maximum ET of about 1100 mm year^{-1} for locations with an annual rainfall of 3500 mm, and decrease with higher rainfall. These values are generally much lower than ET estimates in other wet forest locations, especially those of tropical or equatorial forests in coastal areas and islands. Studies in wet forests of Puerto Rico (Bruijnzeel, 2002, pers. comm. re: correction of values given by Schellekens et al., 2000) and Fiji (Waterloo et al., 1999), in particular, have found exceptionally high ET rates. These and other prior studies, conducted independently by different researchers using a variety of methods (including eddy covariance, Bowen ratio, temperature variance, canopy water budget—for evaporation of intercepted rainfall, and catchment water balance), give a range of annual ET values from 1048 to 1926 mm for island and coastal sites, up to 75% higher than the highest previous estimates for Hawai'i.

3. Study site

The field site is located at an elevation of 1219 m, in native forest in Hawai'i Volcanoes National Park. Mean annual rainfall is approximately 2500 mm (Giambelluca et al., 1986). The substrate is a tephra deposit derived from an explosive eruption of Kilauea Volcano in 1790 (Wolfe and Morris, 1996). Soil is a medial silt loam of the Manu series, classified as ashy, amorphic, isothermic Aquic Hapludands (Natural Resources Conservation Service; http://www.hi.nrcs.usda.gov/soils.html). Soil depth is 40–60 cm, with a bulk density of 0.1–0.6 g cm^{-3} in the upper 5 cm and 0.5–0.8 g cm^{-3} below 5 cm. Saturated hydraulic conductivity varies from about 15 to 50 mm h^{-1} (data provided by P. Niemeyer, NRCS, Hilo). The montane wet forest association present at the study site exemplifies the *Metrosideros/Cibotium* Tree Fern Forest community defined by Gagne and Cuddihy (1999). Vegetation is dominated by a nearly monotypic overstory of *Metrosideros polymorpha* (approximately 2050 individuals greater than 5 cm DBH/ha) with an understory of tree fern, *Cibotium glaucum* (1650 individuals/ha; Table 1). *Ilex anomala* is also present and is considered the second-most abundant canopy tree species in the area by Stone and Pratt (1994). *Myrsine lessertiana* and *Coprosma ochracea* are sub-canopy species with approximately equal, but relatively sparse representation. The tower location was selected after consideration of fetch

Table 1 – Characteristics of the dominant stand species *Metrosideros polymorpha* and *Cibotium glaucum*

	M. polymorpha	*C. glaucum*
Stem density (ha^{-1})	2050	1650
Height (m)	14.5 ± 1.4	3.8 ± 2.7
Projected leaf area index, LAI[a]	4.8 ± 0.5	1.3 ± 0.4
Above ground biomass[b] (Mg C ha^{-1})	109.0 ± 9.4	17.7 ± 5.1

Height, LAI, and biomass values given as mean plus or minus the standard deviation.

[a] LAI estimated for *Metrosideros* based on LAI-2000 (LiCor Inc., Lincoln, NE, USA) plant area index measurements with an estimated stem silhouette area index value of 0.3 (based on LAI-2000 measurements for defoliated *Metrosideros*) subtracted; *Cibotium* LAI based on Harrington et al. (2001).

[b] Biomass calculated for *Metrosideros* with relationship provided by Raich et al. (1994) using stem diameter at breast height measurements from ground survey and tree height measurements from Carnegie Airborne Observatory (CAO) airborne LIDAR measurements; biomass for *Cibotium* calculated from U.S. Forest Service estimate of 17.3 kg per individual for ferns between 2 and 4 m in height.

implications. Winds at the site are persistently from the NNE (between 0° and 60° more than 80% of the time), and our native forest stand extends more than 700 m in that direction. Based on the method of Schuepp et al. (1990, Eq. (13), p. 366), under typical conditions of 4.6 m s^{-1} wind speed and 0.57 m s^{-1} friction velocity, approximately 92% of fluxes measured at the tower are derived from the upwind area within 700 m of the tower and 80% are derived from the area within 280 m. Based on that analysis, fetch is adequate for eddy covariance measurements in all directions except to the W and SW, where it is limited to 400–550 m by Klauea Iki Crater. W and SW winds are not common at the site.

4. Methods

The overall approach of this study is based on measurement of the major components of energy and water exchange at the site. The energy balance can be described using the law of conservation of energy applied to an area of the earth's surface as

$$R_{net} - LE - H - G - S_{biomass} - S_{air} - Q = 0 \quad (1)$$

where R_{net} = net radiation, LE = latent heat flux to the atmosphere, H = sensible heat flux to the atmosphere, G = sensible heat flux to the soil, $S_{biomass}$ = change in stored sensible energy in the biomass, S_{air} = change in stored sensible and latent energy in the air between the eddy covariance sensors and the ground, and Q = the sum of all other sources and sinks (Wilson et al., 2002). All terms in Eq. (1) can be expressed in units of W m^{-2}. In this study, R_{net}, LE, H, G were measured, $S_{biomass}$ and S_{air} were estimated from measurements of air temperature and humidity and biomass temperature. The Q term was assumed to be negligible.

4.1. *Eddy covariance measurements and flux estimation*

A three-dimensional sonic anemometer (model CSAT3, Campbell Scientific, Logan, UT, USA) and an open-path infrared gas analyzer (IRGA, model LI-7500, LiCor, Lincoln, NE, USA) installed at a height of 25 m, approximately 8 m above the canopy, were used to estimate LE and H via the eddy covariance (EC) technique. In addition to consideration of upwind stand homogeneity, the site was selected because of its low topographic slope in the principal upwind direction to minimize terrain-related influences on ET (Huntingford et al.,

Table 2 – Field instrumentation

Component	Model	Vertical level (m)	Measured variables[a]
3D sonic anemometer	CSAT3[b]	25	U_x, U_y, U_z, T_{sonic}, P
Infrared gas analyzer	LI-7500[c]	25	H_2O, CO_2
Pyranometer	8-48[d]	26	K_d
Quantum sensor	LI-190SB[c]	26	PAR
Net radiometer	Q*7[e]	25	R_{net}
Net radiometer	CNR1[f]	25	R_{net}
Air temperature/relative humidity sensor	HMP45C[g]	25	T_{air}, RH
Air temperature sensors (3)	TT-T-24-SLE[h]	3	T_{air}
		9	T_{air}
		15	T_{air}
Biomass temperature sensor (20)	TT-T-24-SLE[h]	0.5	$T_{biomass}$
		3	$T_{biomass}$
		9	$T_{biomass}$
		15	$T_{biomass}$
Soil heat flux transducer (4)	HFT-3[e]	−0.08	SHF
Averaging soil temperature probe (2)	TVAR[b]	−0.02 and −0.06	T_{soil}
Raingage (2)	TE525[i]	18	RF
Soil moisture probe (3)	CS615[b]	−0.04	θ_1
		−0.21	θ_2
		−0.34	θ_3
Data logger	CR5000[b]		

[a] U_x, U_y, U_z = x, y, and z components of wind velocity, T_{sonic} = air temperature derived from speed of sound, P = air pressure, H_2O = water vapor concentration, CO_2 = carbon dioxide concentration, K_d = solar radiation, PAR = photosynthetically active radiation, R_{net} = net radiation, T_{air} = air temperature, RH = relative humidity, $T_{biomass}$ = biomass temperature, SHF = soil heat flux, RF = rainfall, θ_1, θ_2, θ_3 = volumetric soil moisture content at depths 1, 2, 3.
[b] Campbell Scientific, Logan, UT, USA.
[c] LI-COR, Lincoln, NE.
[d] Eppley Laboratory, Newport, RI, USA.
[e] Radiation and Energy Balance Systems, Seattle, WA, USA.
[f] Kipp & Zonen, Delft, The Netherlands, used for post calibration of the Q*7.
[g] Vaisala, Helsinki, Finland.
[h] Thermocouples fabricated from Omega Engineering thermocouple wire.
[i] Texas Electronics, Dallas, TX, USA.

1998). Direct estimates of all energy balance components allow the reliability of flux measurements to be evaluated by checking energy balance closure. The tower instrumentation is listed in Table 2.

Before calculating fluxes, raw 10-Hz data were filtered to remove spikes, and to screen out out-of-range values for each variable, high-moment statistics were evaluated to detect possible sensor or logger malfunctions, and discontinuities were detected and removed. For each 30-min period, means and standard deviations of wind (U_x, U_y, U_z) and sonic temperature (T_{sonic}) from the CSAT3, water vapor (H_2O), carbon dioxide concentration (CO_2), and air pressure (P) from the LI-7500, and air temperature (T_{air}) and vapor pressure (e; derived from T_{air} and RH) from the HMP45C were computed after removing out-of-range data points. For each variable x, data points (x_i) for which $x_i > \bar{x} + 6\sigma$ or $x_i < \bar{x} - 6\sigma$ were identified as spikes and replaced with $\bar{x}$. Means and standard deviations were recalculated after removing spikes. The coordinate system for the three dimensional wind velocity variables was rotated, first around the z-axis, then around the y-axis, according to the method of Tanner and Thurtell (1969) (also see Wilczak et al., 2001), so that the mean wind direction in each 30-min period lies along the x-axis and the mean vertical velocity was forced to zero. LE, H, and carbon dioxide flux (F_{CO_2}) were computed using the covariances of the rotated 10-Hz vertical wind velocity with the 10-Hz water vapor concentration, sonic temperature, and carbon dioxide concentration, respectively. Fluxes were corrected for density effects (Webb et al., 1980). Using sample 30-min intervals during each month of the study period, including early morning, mid-morning, afternoon, evening, and late night periods, the water vapor spectrum and the cospectra of water vapor and vertical wind velocity were evaluated using the method of Högström et al. (1989) (also see Goulden et al., 1996). Spectral losses were found to be negligible, ranging from 0 to 1.5% for water vapor flux, with typical losses near 0.5–0.6%. No corrections were applied for spectral loss. Our code to analyze the EC data was based in part on that of Noormets et al. (2007) and Baldocchi et al. (1988).

The 30-min fluxes were filtered so that periods were included only if (a) wind direction was 0–110° or 315–360°, which excludes periods with wind trajectories disturbed by tower and sensor interference and trajectories over heterogeneous land cover and/or rough terrain; (b) friction velocity was greater than a threshold of 0.22 m s^{-1} (determined based on the method described by Saleska et al. (2003) and Miller et al. (2004)); (c) energy closure error (ECE), defined as

$$\mathrm{ECE} = R_{net} - G - \mathrm{LE} - H \tag{2}$$

was between −200 and 400 W m^{-2}. For statistical analysis involving comparison among energy terms, periods were excluded if any energy term was missing. Both the sonic anemometer and the IRGA output diagnostic indices, "csat-warning" and "agc", respectively. The csat-warnings are triggered by detection of abrupt changes in sonic temperature, poor signal lock, sonic signal higher or lower than expected amplitude range, all of which can be caused by an obstruction in the anemometer path (Campbell Scientific Inc., 1998). The agc variable indicates the optical clarity of the sensor window and responds to the presence of water droplets (LI-COR Inc., 2004). We found these variables to be valuable indicators of wet sensor conditions. Both instruments perform poorly when the sensing surfaces are wet. A csat-warnings value >0 (for the sonic anemometer) and an agc value >50, were found to be consistent indicators of sensor wetting. Thirty-minute periods were therefore excluded when either or both of these variables exceeded their respective thresholds. Lastly, limited manual screening of outlier points was done for each of the 30-min flux time series.

4.2. Net radiation

Accurate measurement of R_{net} is critically important for testing and interpretation of EC flux estimates. REBS (Radiation Energy Balance Systems Inc.) net radiometers are widely used in similar applications (Field et al., 1992). Older REBS models have been shown to significantly underestimate R_{net} (Hodges and Smith, 1997). In our case, a relatively recent model (Q*7.1) REBS sensor was utilized, and recommended daytime and nighttime calibrations and wind corrections were employed. We later installed a Kipp & Zonen CNR1 (The Netherlands) net radiometer along side the REBS sensor and found that the REBS measurements underestimated the Kipp & Zonen values by slightly less than 1% during the day (when $R_{net} > 0$), and by 45% at night. Based on a comparison with a four-way directional reference system traceable to a primary standard,[1] Hodges and Smith (1997) found that the REBS Q*6 net radiometers they tested consistently underestimated R_{net} by around 5 and 45% for daytime and nighttime, respectively. With slopes derived from least-squares regression and using the Kipp & Zonen sensor as a standard, our REBS measurements were post-calibrated by factors of 1.0087 ($r^2 = 0.994$, $N = 329$) and 2.2462 ($r^2 = 0.899$, $N = 337$) for daytime and nighttime periods, respectively. Following adjustment, the R_{net} estimate had a standard error of 14.9 W m^{-2} (11% of the mean).

4.3. Soil heat flux

Using output from four soil heat flux plates (model HFT-3, Campbell Scientific) placed at a depth of 8 cm, two 4-probe averaging soil temperature sensors installed at depths of 2 and 6 cm, and a soil moisture reflectometer (model CS-616, Campbell Scientific) at a depth of 4 cm, we estimated the 30-min time series of soil heat flux as

$$\begin{aligned} G &= F + M, \\ F &= \frac{\mathrm{SHF}_1 + \mathrm{SHF}_2 + \mathrm{SHF}_3 + \mathrm{SHF}_4}{4}, \\ M &= \frac{\mathrm{d}T_{soil}}{\mathrm{TI}} D(\rho_b C_s + \rho_w \theta C_w) \end{aligned} \tag{3}$$

where G = soil heat flux at soil surface (W m^{-2}), SHF_j = soil heat flux (W m^{-2}) at 8 cm, average of four sensors, $\mathrm{d}T_{soil}$ = change in

[1] An Eppley (Eppley Laboratory, Inc., Newport, RI, USA) pyranometer–pyrgeometer system composed of a precision spectral pyranometer (PSP) and a precision infrared radiometer (PIR) were calibrated by Eppley Laboratory. These sensors were subsequently used to field calibrate another Eppley PSP/PIR pair to provide the four-way directional reference system.

temperature in upper 8-cm soil layer during time interval (K), average of two sensors, TI = time interval = 1800 s, D = depth of layer above soil heat flux plates (0.08 m), ρ_b = soil bulk density (kg m^{-3}), C_s = specific heat for mineral soil (J kg^{-1} K^{-1}), ρ_w = density of water = 1000 kg m^{-3}, θ = volumetric soil moisture content (m^3 m^{-3}), and C_w = specific heat for water (J kg^{-1} K^{-1}). The correction for heat flux plate measurements proposed by Philip (1961) was found to produce negligible results in this case and was therefore not applied.

4.4. *Energy storage in the biomass and air beneath EC sensors*

Energy storage in the biomass was evaluated using measured or estimated temperature fluctuations in tree and tree fern stems and leaves, epiphytes, and litter. Sensors were inserted into holes drilled at three levels (3, 9 and 15 m) in a representative *Metrosideros* tree. At each level, four thermocouples were installed around the circumference of the stem at the four cardinal directions, at a 1-cm depth, and one sensor was placed on the north side of the tree at a depth of 3 cm. The 12 sensors placed at 1 cm depth were assumed to be representative of the outer 1.5 cm of all tree and branch biomass, while the deeper sensors were representative of the rest of the tree biomass. Four thermocouples were similarly placed at 1.5 cm depth in a *Cibotium* stem at its midpoint height (0.5 m), and one sensor was placed at 4.5 cm depth on the north side of the tree fern. The four sensors placed at 1.5 cm depth were assumed representative of the outer 3 cm of all tree fern stem biomass, while the deeper sensors were representative of the rest of the tree fern stem biomass. Canopy leaf temperature was determined from upward longwave radiation measured by the CNR1 net radiometer mounted on the tower, using the Stefan–Boltzmann equation with an assumed emissivity of 0.975. The temperature of litter and epiphytes was assumed equal to that of the outer *Cibotium* stem.

The biomass of stems and leaves of *Metrosideros*, *Ilex*, and *Coprosma* were determined using a survey of DBH (diameter at breast height) in a 20 m × 20 m plot near the measured trees and allometric equations developed by Raich et al. (1997). Heights of trees in the plot were determined from DBH/height relationships constructed in the general vicinity. Average ratios of wet to dry biomass for the above species were obtained from Aplet and Vitousek (1994). *Cibotium* stem biomass was based on the calculation of volume from field measurements of midpoint stem diameter and stem height in the 20 m × 20 m plot, assuming a cylindrical shape. The density of live *Cibotium* stems was estimated to be 1.0 g cm^{-3}. *Cibotium* leaf biomass was estimated from the average ratio of leaf biomass to stem biomass found in all trees in the plot.

Litter biomass was determined from the average mass of twelve 0.5 m^2 samples of all surface litter, weighed immediately after collection. Fallen dead-wood biomass was estimated from volume calculations determined by a survey at the field site. The wet density of fallen dead wood was estimated to be 1.2 g cm^{-3} based on a bulk density for dry dead wood of 0.24 g cm^{-3} (Sandström et al., 2007) and a 5:1 wet- to dry-weight ratio, based on the observed field mass and dry mass of our litter samples. Epiphyte wet biomass was obtained from a survey of all epiphytes in the same 20 m × 20 m plot including the water mass of samples (Mudd, 2004).

Using these methods, wet biomass estimates for the inner and outer portions of the woody parts of canopy trees were 44.79 and 24.12 kg m^{-2}, respectively. For *Cibotium*, the wet biomass was 2.67 and 1.68 kg m^{-2}, respectively, for inner and outer portions. Wet biomass of the leaves of the main canopy trees was estimated to be 2.67 kg m^{-2} using equations of Raich et al. (1997). Wet biomass of *Cibotium* leaves was estimated to be 0.21 kg m^{-2}, and thus estimated total leaf wet biomass was 2.88 kg m^{-2}. Litter wet biomass (including fallen dead wood) was estimated to be 8.29 kg m^{-2}, while epiphytes contributed another 0.39 kg m^{-2}.

For each 30-min interval, the change in stored sensible energy in the biomass ($S_{biomass}$; W m^{-2}) was estimated as

$$S_{biomass} = \sum \frac{dT_{biomass\,i}}{dt}(C_i BM_i) \tag{4}$$

where the index i represents the different elements of above-ground biomass considered in this study, $dT_{biomass\ i}$ = change in temperature of biomass type i during time interval (K), dt = length of time interval = 1800 s, C_i = specific heat of the relevant biomass type (J kg^{-1} K^{-1}; value based on Wilson and Baldocchi, 2000), and BM_i is the wet biomass of each above-ground biomass element (kg m^{-2}).

Shielded thermocouples were placed at heights of 3, 9, and 15 m on the tower. Together with the temperature/humidity sensor (HMP45C; see Table 2) at the top of the tower, these sensors provide a measure of the variation in temperature of the air layer below the EC sensors. Humidity measurements at the top of the tower were used to represent changes in humidity in the layer below the sensors (no humidity measurements were made below the top of the tower). For each 30-min interval, the change in stored sensible and latent energy in the air layer (S_{air}; W m^{-2}) was estimated as

$$S_{air} = z\frac{dT_{air}}{dt}[(C_p\rho_{dry_air}) + (C_{wv}q)] + z\frac{dq}{dt}\lambda \tag{5}$$

where z = depth of the air layer (25 m), dT = change in mean air layer temperature during time interval, dt = length of interval = 1800 s, C_p = specific heat of dry air at constant pressure = 1004 J kg^{-1} K^{-1}, ρ_{dry_air} = dry air density (kg m^{-3}), C_{wv} = specific heat of water vapor (J kg^{-1} K^{-1}), q = water vapor density (kg m^{-3}), and λ = latent heat of vaporization (J kg^{-1}, estimated as a function of air temperature).

Installation of both biomass and air temperature sensors at the site was not completed until after the study period reported here. Therefore, we used the mean diurnal cycle of $S_{biomass}$ and S_{air} based on measurements taken at the site during March–August 2007 in subsequent analysis of energy closure during February 2005 to February 2006.

4.5. *Canopy conductivity*

To assess the physiological control over water losses, canopy conductance (g_c) was estimated by inverting the Penman–Monteith equation (Monteith, 1973) to solve for g_c, and using measured LE, air temperature, humidity, R_{net}, and wind speed.

4.6. *Mean diurnal cycle and monthly mean*

For each measured or derived time series, the monthly mean diurnal cycle was calculated by obtaining the mean value for each 30-min time interval of the day (48 intervals) for a given month. Intervals with no good data during a month or with a coefficient of variation greater than 20 were coded as missing. The monthly mean 30-min values were further processed by gap filling and smoothing. First, any missing points were interpolated from adjacent points for gaps of one or two intervals. For gaps of three or more consecutive intervals, values from corresponding intervals in the previous month were substituted. Once all 48 intervals are filled, a finite impulse response low-pass filter (Jackson, 1996), based on the Kaiser window function (Kaiser, 1966), was used to remove high frequency variations in the diurnal cycle. Each mean monthly value was computed as the average of the resulting 48 values in the smoothed mean diurnal cycle.

5. Results

5.1. *Temporal variation in meteorological and flux variables*

Observed time series of daily rainfall, wind speed, R_{net}, vapor pressure deficit (VPD), air temperature (T_{air}), and soil moisture (θ) at three depths are shown in Fig. 1. The rainfall distribution

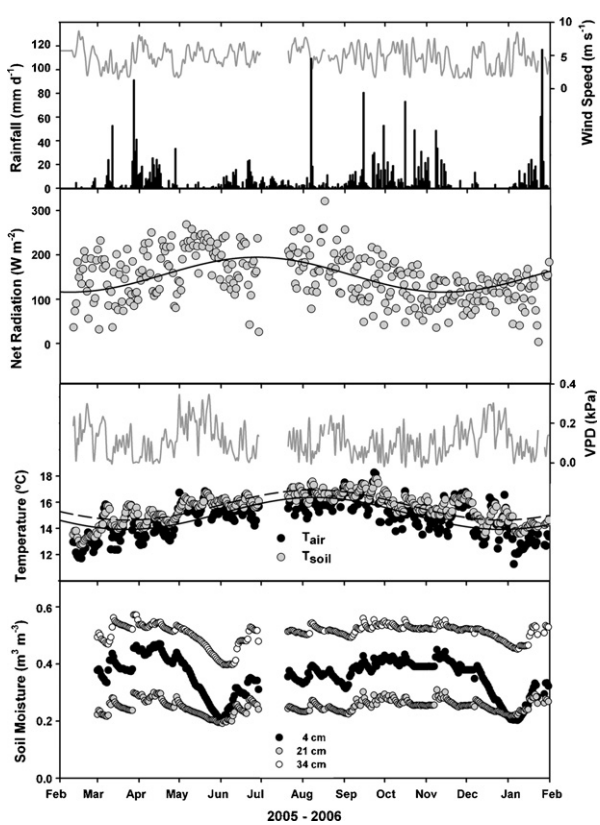

Fig. 1 – Time series of daily rainfall, wind speed, net radiation, vapor pressure deficit (VPD), air temperature, and soil moisture.

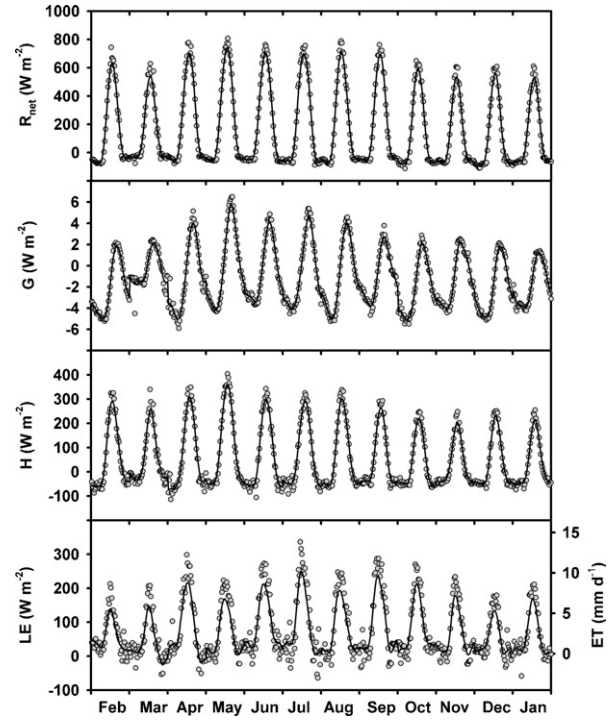

Fig. 2 – Diurnal cycles by month of net radiation, soil heat flux, sensible energy flux to the atmosphere, latent energy flux, and evapotranspiration. Symbols give 30-min means; line is smoothed using a finite impulse response low-pass filter (Jackson, 1996).

is punctuated by distinct dry periods, during February, May, and December of 2005. The latter two periods are marked by deep drawdowns in soil moisture, especially in the surface layer. The effects of reduced rainfall during these periods are also seen in the form of higher VPD. The R_{net} cycle follows the expected pattern based on changing sun angle, with the maximum and minimum near the solstices. T_{air} lags the radiation cycle by about 2–3 months.

The mean diurnal cycles of the energy components, derived for each month, are shown in Fig. 2. The net radiation pattern reflects the seasonally and diurnally changing sun angle and day length. G, H, and LE generally respond to net radiation, although the partitioning between H and LE is further modulated by other factors, such as leaf area index (LAI) and water availability.

5.2. *Energy storage terms*

The mean diurnal cycle of soil heat flux over the whole study period ranged from $-4.1\,W\,m^{-2}$ (7:00 a.m.) to $3.0\,W\,m^{-2}$ (4:00 p.m.). The mean diurnal cycles of air layer and biomass energy storage terms, for the period March–August 2007, are shown in Fig. 3. Of the eight individual aboveground energy storage components evaluated, the inner and outer main canopy tree stem elements have the largest amplitudes, with ranges of -14 to $24\,W\,m^{-2}$ and -12 to $18\,W\,m^{-2}$, respectively. Changes in sensible and latent energy storage due to fluctuations in the temperature and humidity of the canopy

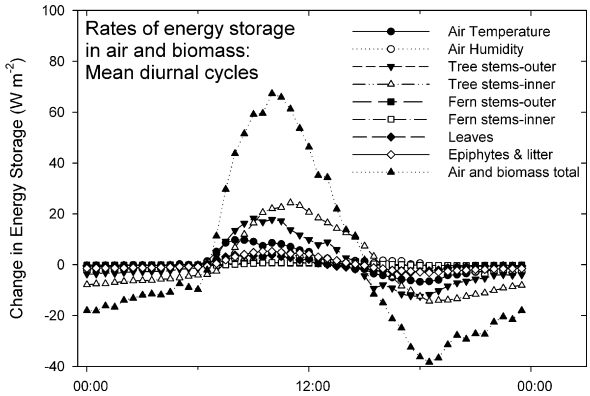

Fig. 3 – Mean diurnal cycles of energy storage flux in air and biomass at the study site during March–August 2007.

air layer account for energy fluxes of −7 to 10 W m^{-2} and −4 to 5 W m^{-2}, respectively. The combined air and biomass energy storage rate ranges from −38 to 67 W m^{-2}. These results are reasonable in comparison with smaller fluxes found in 12-m pine forest (Meesters and Vugts, 1996) and somewhat large fluxes found in 30-m Amazonian rainforest (Moore and Fisch, 1986) and 25-m Eucalyptus forest in Western Australia (Silberstein et al., 2001). Because air and biomass energy storage measurements were not taken during the 2005–2006 study period, the mean diurnal cycle from the 2007 data was used in the evaluation of energy balance closure.

5.3. *Energy balance closure*

To evaluate the EC estimates of LE and H, we examined the energy balance by plotting 30-min values of $\mathrm{LE}+H$ vs. $R_{\mathrm{net}}-G-S_{\mathrm{biomass}}-S_{\mathrm{air}}$ (Fig. 4), and by computing the energy closure ratio (ECR):

$$\mathrm{ECR}=\frac{\overline{\mathrm{LE}}+\overline{H}}{\overline{R}_{\mathrm{net}}-\overline{G}-\overline{S}} \tag{6}$$

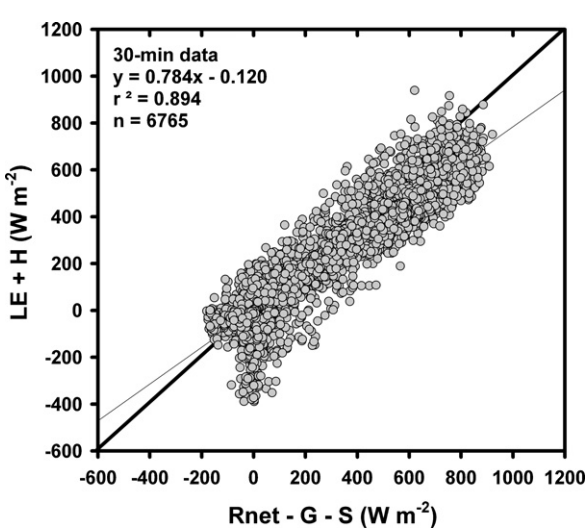

Fig. 4 – Energy balance scatter plot showing degree of energy balance closure based on 30-min data.

Table 3 – Energy balance closure statistics.

	ECR[a]	Slope	Intercept	r^2
This study				
February	0.752	0.734	3.30	0.877
March	0.763	0.815	−11.46	0.877
April	0.797	0.808	−3.76	0.874
May	0.780	0.809	−7.94	0.922
June	0.788	0.808	−5.40	0.901
July	0.810	0.788	6.15	0.884
August	0.767	0.788	−4.75	0.922
September	0.761	0.801	−9.37	0.867
October	0.825	0.786	6.98	0.876
November	0.837	0.778	8.58	0.883
December	0.760	0.700	9.67	0.868
January	0.785	0.781	0.79	0.877
Annual	0.784	0.784	−0.12	0.894
FLUXNET sites (Wilson et al., 2002)				
Minimum	0.34	0.55	−32.9	0.64
Maximum	1.69	0.99	36.9	0.96
Mean	0.835	0.785	3.74	0.862

[a] Energy closure ratio.

where overbars indicated means over the 1-year study period. Table 3 gives the slope, intercept, and r^2 value, obtained by ordinary least-squares regression, and ECR for our site, in comparison with minimum, maximum, and mean values from sites in the FLUXNET system (Wilson et al., 2002). Annual ECR and slope obtained here (both equal to 0.784) are slightly below the respective means, but well within the range of values found at the FLUXNET sites. Energy closure error has numerous possible sources. Wilson et al. (2002) identify and discuss various suspected sources of error. Measurement bias in available energy variables, especially R_{net}, has been cited as a possible contributor to energy closure error at other sites (Halldin and Lindroth, 1992). However, R_{net} measurements are probably the most accurate of the major components of the energy balance (Twine et al., 2000) and tend to be biased on the low side (Hodges and Smith, 1997), which would not explain low values of ECR. Cross-checking and adjustment of our REBS-based R_{net} measurements using the Kipp & Zonen instrument adds confidence to these measurements. Soil, air, and biomass storage terms are accounted for in our study. Further, heat storage averages close to zero over the diurnal cycle, and therefore is unlikely to significantly affect ECR. Therefore, it is plausible that the energy closure error is mainly due to an underestimate of LE and H. Twine et al. (2000) recommended closing the surface energy balance by the "Bowen-ratio closure" method, which assumes that LE and H are the sources of closure error, but that the Bowen ratio ($\beta = H/\mathrm{LE}$) is correctly estimated. Adopting this method would imply that the true values of LE and H in our study are higher by a factor of $\mathrm{ECR}^{-1} = 1.276$.

5.4. *Mean monthly ET and related variables*

Monthly mean values of ET and relevant meteorological and surface variables are given in Table 4. Rainfall for the 12-month study period (2401 mm) is slightly below the mean annual rainfall (2500 mm), but is highly variable from month

Table 4 – Mean monthly meteorology, energy balance, and evapotranspiration during study period

	Month												
	February 2005	March 2005	April 2005	May 2005	June 2005	July 2005	August 2005	September 2005	October 2005	November 2005	December 2005	January 2005	Annual
Rainfall (mm)	35.8	310.0	263.3	22.8	186.5	103.4	185.8	355.4	347.4	208.3	29.9	352.4	2401.0
Solar radiation (W m^{-2})	227.9	191.4	264.5	292.6	275.8	273.7	256.3	249.6	214.3	185.3	199.4	187.5	234.9
PAR (μmol s^{-1} m^{-2})	463.3	386.7	540.6	599.9	555.9	556.6	520.9	487.7	420.4	365.6	390.9	368.5	471.4
Net radiation (W m^{-2})	153.7	145.4	203.8	219.4	205.7	202.0	192.2	188.6	138.9	116.5	112.7	119.0	166.5
Mean T_{air} (°C)	12.6	14.0	13.8	15.8	15.6	16.2	16.1	16.5	15.1	15.1	14.4	13.1	14.8
Minimum T_{air} (°C)	10.9	12.6	11.6	13.5	13.7	14.2	14.0	15.0	13.5	13.7	12.5	11.7	13.1
Maximum T_{air} (°C)	15.5	16.5	16.5	19.0	18.3	18.9	19.1	18.9	17.6	17.5	17.2	15.3	17.5
T_{soil} (0–8 cm layer; °C)	13.3	14.8	14.7	16.0	16.0	16.8	16.6	16.9	15.9	15.7	15.0	14.2	15.5
VPD (kPa)	0.171	0.159	0.132	0.225	0.151	0.153	0.171	0.142	0.164	0.147	0.217	0.126	0.163
Wind speed (m s^{-1})	5.7	3.2	5.3	4.9	5.4	5.8	4.7	5.1	4.9	4.4	4.8	4.9	4.9
θ at −0.04 m (m^3 m^{-3})		0.391	0.439	0.313	0.289	0.350	0.359	0.382	0.405	0.402	0.319	0.255	0.355
θ at −0.21 m (m^3 m^{-3})		0.249	0.275	0.223	0.233	0.241	0.245	0.258	0.267	0.265	0.245	0.246	0.250
θ at −0.34 m (m^3 m^{-3})		0.522	0.531	0.476	0.455	0.511	0.516	0.520	0.530	0.527	0.503	0.483	0.506
ET (mm)	59.9	48.3	91.7	81.2	102.8	106.8	89.7	100.7	93.1	68.0	56.9	66.8	965.8
ECR	0.752	0.763	0.797	0.780	0.788	0.810	0.767	0.761	0.825	0.837	0.760	0.785	0.784
ET/ECR (mm)	79.7	63.3	115.1	104.1	130.6	131.9	116.8	132.3	112.8	81.2	74.9	85.0	1232.1
Mean daytime g_c	0.0123	0.0124	0.0267	0.0128	0.0290	0.0245	0.0193	0.0293	0.0334	0.0219	0.0113	0.0240	0.0214

Note: PAR = photosynthetically active radiation; T_{air} = air temperature; T_{soil} = soil temperature; VPD = vapor pressure deficit; θ = volumetric soil moisture; ET = evapotranspiration; ECR = energy closure ratio; g_c = canopy conductance.

to month, with order-of-magnitude differences between consecutive months occurring several times. Monthly solar radiation (K_d), photosynthetically active radiation (PAR), and R_{net} all peak in May, with minima in November (K_d and PAR) and December (R_{net}). As seen in Fig. 1, temperature lags the radiation cycle with minimum and maximum in February and September, respectively. VPD remains fairly constant throughout the year except for significant peaks in May and December, corresponding to periods of low rainfall. Soil moisture in all layers is highest in April. Minimum soil moisture occurs in January, May, and June for layers 1, 2, and 3, respectively. ET is lowest in March and highest in July. Canopy conductivity is lowest in December and highest in October.

6. Discussion

6.1. *Comparison with previous ET estimates*

Our annual ET estimate, unadjusted and with the Bowen-ratio closure adjustment, is shown in Table 5 along with prior ET estimates in Hawai'i and other similar study sites. With the Bowen-ratio closure adjustment, the current estimate is about 40% higher than previous estimates for similar sites in Hawai'i, and approaches levels found for lowland rainforest in Amazonia with similar annual rainfall (RF = 2636 mm, ET = 1319 mm; Shuttleworth, 1988). Note that ET generally amounts to around 80% of rainfall at tropical and equatorial maritime sites, with the 7–12-m montane cloud forest in Jamaica (Hafkenscheid et al., 2002) being a notable exception (Table 5). Prior ET estimates for Hawai'i were only around 35–40% of rainfall, while the current ET estimate is at 51% of rainfall. Some uncertainty remains in the upward adjustment used to achieve energy closure (Massman et al., 2003), and hence this estimate must be used with caution. If proven to be accurate, however, the annual ET rate of 1232 mm represents a significant increase over previous estimates in Hawai'i, with implications for prior groundwater recharge estimates made with lower ET estimates.

6.2. *ET diurnal variation*

ET and each of the energy balance components exhibit distinct diurnal cycles (Fig. 2). The diurnal variation in ET roughly follows the diurnal R_{net} cycle, but the response is attenuated by changes in water availability, as indicated by variations in canopy conductance. Fig. 5 shows the mean diurnal cycles of daytime (08:00–17:00) g_c for each month. In general, g_c is highest in the morning, drops steadily to a minimum value in mid- to late-afternoon, then, in some months, recovers somewhat before sundown. This pattern suggests that stomatal control increases with evaporative demand. Midday stomatal closure is a well-known phenomenon in which, despite abundant available water in the root zone, plant stomata progressively restrict gas exchange as stem and tissue water storage is depleted during the day. A possible contributing effect may result from a tendency for plant leaves to be wet in the morning, as a result of rain, fog, or dew deposition during the night. If wet canopy evaporation rates are higher than evapotranspiration under dry canopy conditions, we would expect g_c to be high in the morning and decrease as the canopy dries. Relative rates of wet canopy evaporation and dry canopy ET are discussed further below.

Table 5 – Summary of tropical and equatorial forest rainfall and evapotranspiration estimates (annual values)

Site	RF (mm)	ET (mm)	ET/RF
Tropical maritime—Hawai'i (this study)			
Hawai'i	2401	966	0.402
Hawai'i[a]	2401	1232	0.513
Tropical maritime—Hawai'i (prior studies)			
Hawai'i[b]	2480	870	0.351
Hawai'i[c]	2000	810	0.405
Hawai'i[c]	2500	898	0.359
Hawai'i[d]	3000	1047	0.349
Mean	2495	906	0.366
Tropical maritime—other than Hawai'i			
Fiji[e]	2054	1926	0.938
Fiji[f]	2054	1717	0.836
Puerto Rico[g]	1473	1219	0.828
Jamaica[h]	3060	1048	0.342
Queensland, Australia[i]	1311	1259	0.960
Mean	1990	1434	0.781
Equatorial maritime			
Peninsular Malaysia[j]	1571	1448	0.922
Borneo[k]	2151	1545	0.718
Mean	1861	1497	0.820
Equatorial continental			
Amazonas, Brazil[l]	2636	1319	0.500
Amazonas, Brazil[m]	2089	1123	0.538
Pará, Brazil[n]	1550	1516	0.978
Rondônia, Brazil[o]	2200	1359	0.618
Guyana[p]	2700	1520	0.563
Mean	2235	1367	0.674

[a] This study, with Bowen-ratio closure adjustment.
[b] Carrillo (pers. comm., 2002).
[c] Giambelluca (1986).
[d] Derived from analysis reported by Giambelluca et al. (1996).
[e] Waterloo et al. (1999); 6-year-old pine.
[f] Waterloo et al. (1999); 15-year-old pine.
[g] Van der Molen (2002).
[h] Hafkenscheid et al. (2002).
[i] Hutley et al. (1997).
[j] Tani et al. (2003).
[k] Kumagai et al. (2005).
[l] Shuttleworth (1988).
[m] Malhi et al. (2002).
[n] Jipp et al. (1998).
[o] von Randow et al. (2004).
[p] Jetten (1994), reported by ter Steege et al. (1995).

6.3. *ET variation: dry and wet periods*

Month-to-month variability of rainfall and ET is evident in Table 4. Despite the high annual rainfall at the site, some months during the study period are quite dry. We identified four distinct dry periods and three wet periods, and derived

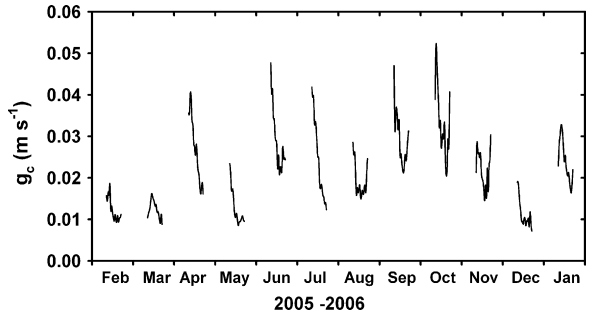

Fig. 5 – Diurnal cycle of canopy conductivity by month.

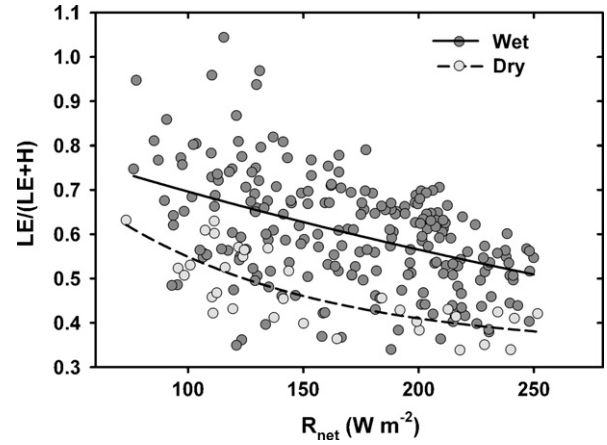

Fig. 6 – Daily LE/(LE + *H*) vs. net radiation (R_{net}) for wet and dry days.

mean values of ET and related variables (Table 6). ET is higher in all three wet periods than any of the dry periods. Using the period averages in Table 6, variations in soil moisture among the periods do not appear to be related to ET variations. However, ET variations do correspond with variations in rainfall, PAR, R_{net}, mean and minimum air temperature, VPD, wind speed, and soil temperature. Hence, the observed higher ET during wet periods does not necessarily result primarily from higher soil moisture availability.

6.4. *Energy partitioning*

To assess how energy is partitioned under different conditions, daily values of LE as a fraction of turbulent energy flux (LE + *H*) are plotted against R_{net} in Fig. 6. Days with and without rainfall are differentiated. In both cases, the fraction of energy used for ET decreases as R_{net} increases. The fact that a smaller proportion of energy is used for ET on days with high available energy, implies that resistance to flow within the soil–plant continuum increases in response to higher evaporative demand. This is in agreement with diurnal response to increasing demand, as seen in the diurnal cycle in g_c (Fig. 5). Soil–plant water flow resistance limits transpiration, but has no effect on evaporation from plant and litter surfaces wetted by rain, fog, or dew. However, the apparent resistance increases with R_{net} for both dry and wet days, indicating that transpiration is contributing significantly to stand ET on wet days. It is also clear that the proportion of energy devoted to ET is higher for wet days. At the same level of R_{net}, energy devoted to ET is, on average, approximately 29% higher on days with rain, than on days without rain. Given this enhanced ET during wet canopy periods and the high frequency of canopy wetting by rain and fog, it is apparent that evaporation of intercepted rainfall, and perhaps fog, is an important component of stand ET at the site.

The fraction of turbulent energy devoted to ET has an annual cycle with a minimum in mid-April and a maximum in mid-October (Fig. 7, top panel). This cycle suggests an annual fluctuation in leaf area, which would be positively correlated

Table 6 – Evapotranspiration and related variables during selected dry and wet periods

Period	Dry				Wet		
	12 February 2005–26 March 2005	29 April 2005–1 June 2005	21 August 2005–1 September 2005	19 November 2005–4 January 2006	27 March 2005–17 April 2005	10 June 2005–27 June 2005	2 September 2005–3 November 2005
N (days)	39	34	12	47	22	18	63
Rainfall (mm day^{-1})	3.3	0.8	3.5	0.9	18.6	7.8	11.8
Solar radiation (W m^{-2})	179.2	266.8	233.7	180.3	181.0	203.2	167.9
PAR (μmol s^{-1} m^{-2})	415.1	595.8	525.7	383.9	509.8	552.8	447.2
Net radiation (W m^{-2})	147.5	219.1	191.4	114.2	192.1	204.6	160.5
Mean T_{air} (°C)	13.6	15.6	16.3	14.8	13.9	15.2	15.7
Minimum T_{air} (°C)	11.5	13.2	14.1	12.4	12.6	13.5	13.9
Maximum T_{air} (°C)	17.1	19.3	19.4	18.3	16.0	17.9	18.1
VPD (kPa)	0.13	0.20	0.16	0.17	0.04	0.07	0.07
Wind speed (m s^{-1})	4.11	4.67	4.30	3.52	5.43	4.99	5.05
Mean T_{soil} (°C)	14.1	16.0	16.5	15.3	14.8	16.0	16.4
θ at −0.04 m (m^3 m^{-3})	0.382	0.318	0.346	0.329	0.450	0.316	0.396
θ at −0.21 m (m^3 m^{-3})	0.243	0.226	0.237	0.246	0.285	0.249	0.263
θ at −0.34 m (m^3 m^{-3})	0.515	0.478	0.511	0.506	0.542	0.480	0.527
ET (mm day^{-1})	1.76	2.62	2.80	1.89	2.90	3.34	3.12

Note: N = sample size; PAR = photosynthetically active radiation; T_{air} = air temperature; VPD = vapor pressure deficit; T_{soil} = soil temperature; θ = volumetric soil moisture; ET = evapotranspiration.

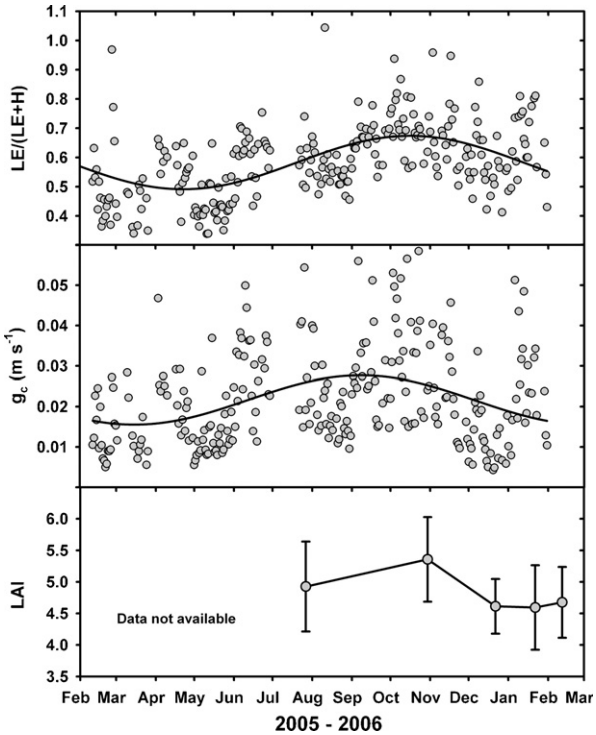

Fig. 7 – Time series of daily LE/(LE + *H*) (top panel), daily canopy conductivity (middle panel), and leaf area index (bottom panel).

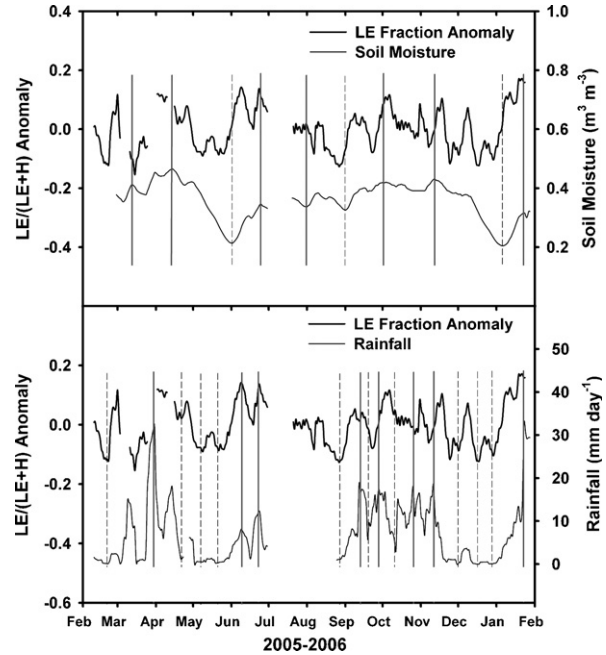

Fig. 8 – Departures of LE/(LE + *H*) from annual cycle (thick black line in both panels) in comparison with soil moisture (thin black line in top panel) and rainfall (thin black line in bottom panel). All three time series are smoothed using 7-day running mean. Solid gray vertical lines identify peaks and dashed lines represent troughs in soil moisture and rainfall.

with both transpiration and wet canopy evaporation. Estimated canopy resistance (Fig. 7, middle panel) and measurements of LAI at the site (Fig. 7, bottom panel) confirm that leaf area fluctuation is in phase with the observed cycle in the proportion of energy devoted to ET.

Daily values of the LE/(LE + *H*) ratio exhibit significant departures from the mean annual cycle (Fig. 7, top panel), with several periods of persistently high or low values. These deviations of energy partitioning from that associated with LAI fluctuation suggest that water availability may be playing a role. In Fig. 8 (top panel), soil moisture is shown in relation to LE/(LE + *H*) anomalies over the course of the observation period. Because of the noisiness of the LE/(LE + *H*) anomalies, both time series are given in the form of 7-day running means, which smoothes out high frequency variations. The comparison indicates a general similarity between the two measures. However, the timing of local minima in energy partitioning and soil moisture are not perfectly in phase. Note that for each of the two large drawdowns in soil moisture, which occurred during May and December–January, the minimum in energy partitioning precedes the soil moisture minimum. If soil moisture were limiting ET, we would expect these minima to coincide closely. In Fig. 8 (bottom panel), 15-day running means of rainfall and LE/(LE + *H*) anomaly are shown. Here we see remarkable coincidence between the two time series, with the two major energy partition minima coinciding precisely with the rainfall minima. This result indicates that periods of low or high rainfall produce an immediate response in the energy partitioning ratio, with lower amounts of energy used for ET during dry periods. Comparing the two graphs in Fig. 8 indicates that ET responds more strongly to current rainfall than to soil moisture, supporting the view that wet canopy evaporation is a major contributor to overall stand ET.

6.5. *Bias due to data rejection: wet sensor problem*

Using EC measurements to estimate fluxes can be especially problematic at sites with frequent rainfall. During the study period, rainfall was observed on 283 of 355 days (79.7%). During periods of rain, fog, or dew deposition, transducer surfaces on the sonic anemometer and sensor windows of the infrared gas analyzer are likely to become wet. Water droplets attenuate the signals for both of these sensors, generating errors. As part of our data screening procedure, errors in wind velocity, sonic temperature, and specific humidity are detected and rejected by several methods. Data screening is vital to producing clean, accurate results, but may introduce biases in averages derived from the selected time intervals. In particular, because sensor wetting is a major cause of data rejection, the screening procedure may bias results by preferentially rejecting periods of high humidity and low solar radiation, conditions associated with wet-instrument periods. The evaporative response to environmental conditions during these wet periods, therefore, may be distinctly different from that during dry periods.

To assess the magnitude of error introduced into averages of LE due to data screening, we first examined the frequency of wet and dry days from the selected ‘‘good data’’ days in comparison with that of the whole record. We used three

different thresholds for the allowable number of missing 30-min intervals to select days for analysis. In all cases, missing intervals were filled with the monthly mean value for that interval. The required number of good 30-min intervals per day was set so that the resulting daily data set was derived from an equal number of good and filled 30-min intervals (the 1:1 data set), twice as many good as filled intervals (2:1), and three times as many good as filled (3:1). Rain occurred on 76.8, 67.2, and 56.6% of days for the 1:1 ($N = 263$ days), 2:1 ($N = 137$ days), and 3:1 ($N = 83$ days) data sets, respectively, in comparison with 79.9% for the whole study period. Hence, as the criterion for including a day in the selection becomes stricter (and the resulting sample becomes smaller), the percentage of wet days decreases. So, while confidence in the individual daily estimates is highest on average for the 3:1 data set, the average is likely to be the most biased due to the disproportionate number of dry days included. The amount of this bias can be estimated by comparing mean ET of the selected days against the weighted average of mean LE for wet and dry days, with weights set according to the proportion of wet and dry days over the whole study year. Doing so results in errors of −0.72, −2.34, and −4.57% for the 1:1, 2:1, and 3:1 data sets, respectively. These results indicate that the bias due to selectively removing wet periods is relatively small.

7. Conclusions

The principal findings resulting from measurements during the 12-month period February 2005 through January 2006 are

1. Total rainfall was close to the long-term mean, but was highly variable from month to month with distinct dry periods in February, May, and December 2005.
2. Measured ET totaled 966 mm for the year, only slightly higher than previous estimates for similar locations in Hawai‘i. But when adjusted following the Bowen-ratio closure approach (Twine et al., 2000), total ET of 1232 mm is significantly higher than previous estimates.
3. Variations in g_c are marked by a diurnal maximum in the morning followed by a steady decline into the afternoon. This pattern suggests that midday stomatal closure is occurring and/or that evaporation is high in the morning because of frequent wet canopy conditions early in the day.
4. The daily fraction of turbulent energy flux used for ET decreases as R_{net} increases, suggesting transpiration is being limited under high evaporative demand conditions.
5. ET is generally higher during rainy periods than dry periods. On the basis of period totals, however, it is not clear whether soil moisture, canopy wetting, temperature, wind, or other variables are responsible for this pattern.
6. On days with rain, the fraction of energy used for ET is, on average, about 29% higher than on dry days. The annual cycle in the fraction of energy used for ET is at a minimum in mid-April and a maximum in mid-October, roughly corresponding to the observed cycle in LAI at the site. Deviations from this cycle appear to correspond more strongly to rainfall than soil moisture, suggesting that canopy wetness is an important control on ET at this wet forest site.
7. Sensor wetting is a significant problem for eddy covariance measurement in high rainfall areas. Rainfall occurred on about 80% of days during the study period, leading to frequent data rejection due to wet sensor-related errors. Analysis suggests that possible biasing due to the preferential rejection of data from wet periods is relatively small.

Our findings have important implications for local hydrological assessment and for understanding the hydrology of wet tropical forests in general. Locally, prior assessments of groundwater recharge developed without any direct ET measurements may have to be revised if further evidence supports the energy closure adjustment at our study site. If confirmed, the adjusted annual ET of 1232 mm at the site is significantly above all previous estimates of forest ET in Hawai‘i and would result in a major revision of groundwater recharge estimates. More broadly, our findings point to the importance of wet canopy evaporation in controlling variations in ET and in contributing to high annual ET in Hawai‘i and similar environments. This highlights the need to focus resources specifically on the measurement of wet canopy processes in tropical forests.

On-going research at the study site will contribute additional information regarding the processes controlling water exchanges in Hawaiian forests. Subsequent papers will present our estimates of transpiration, based on sapflow measurements in the principal canopy and sub-canopy species at the site, and an evaluation of water partitioning in the canopy, based on measurements of rainfall, throughfall, and stemflow. These key additional findings will help to clarify the results presented here and further our understanding of water exchange processes in tropical forests.

A companion study site where the forest has been invaded by an alien tree species was established near the native forest site in 2006. Comparing results from the two sites will allow us to determine the hydrological effects of tree invasion. We will also soon present results of carbon flux and storage at the native and invaded forest sites.

Acknowledgments

This study was made possible through the assistance of many individuals and organizations. The authors especially wish to thank Toby Vana, Harry Buscher, Kim Carlson, Melissa Kunz, Robert Smith, Nick Shema, David Okita, Jon Maka‘ike, Robert Mattos, Todd Tobeck, Tim Tunison, Paul Keali‘iho‘omalu, Michele Montgomery, Patrick Niemeyer, Joseph Conner, and Wanda Martin. We are deeply grateful to Hawai‘i Volcanoes National Park for permitting us to establish the study site within a pristine native forest community in the park. We are grateful to Asko Noormets for allowing us access to his processing code. Special thanks goes to Ed Swiatek (Campbell Scientific Inc.) for his technical advice on tower instrumentation. This project is supported under a collaborative facilities agreement between the Institute of Pacific Islands Forestry (US Forest Service) and the Carnegie Institution of Washington. This paper is based upon work supported by the National Science Foundation under Grant No. EAR-0309731, the endowment of the Carnegie Institution, and by the USGS

Biological Resources Discipline Global Change Research Program.

REFERENCES

Aplet, G.H., Vitousek, P.M., 1994. An age-altitude matrix analysis of Hawaiian rain-forest succession. Journal of Ecology 1, 137–147.

Baldocchi, D.D., Hicks, B.B., Meyers, T.P., 1988. Measuring biosphere-atmosphere exchanges of biologically related gases with micrometeorological methods. Ecology 69, 1331–1340.

Bruijnzeel, L.A., Hamilton, L.S., 2000. Decision time for cloud forests. Humid Tropics Programme Series No. 13. International Hydrological Programme, UNESCO, Paris, 40 pp.

Bruijnzeel, L.A., Wiersum, K.F., 1987. Rainfall interception by a young *Acacia auriculiformis* (A. Cunn.) plantation forest in West Java, Indonesia: application of Gash's analytical model. Hydrological Processes 1, 309–319.

Campbell Scientific Inc., 1998. CSAT3 three dimensional sonic anemometer instruction manual. Campbell Scientific Inc., Logan, UT, USA. Available online: http://www.eol.ucar.edu/rtf/facilities/isff/sensors/csi/csat3/csat3_manual.pdf.

Dykes, A.P., 1997. Rainfall interception from a lowland tropical rain forest in Brunei. Journal of Hydrology 200, 260–279.

Ekern, P.C., 1983. Measured evaporation in high rainfall areas, leeward Ko'olau Range, O'ahu, Hawai'i. Water Resources Research Center Technical Report No. 156. University of Hawai'i, Honolulu, ix + 60 pp.

Field, R.T., Fritschen, L.J., Kanemasu, E.T., Smith, E.A., Stewart, J.B., Verma, S.B., Kustas, W.P., 1992. Calibration, comparison, and correction of net radiation instruments used during FIFE. Journal of Geophysical Research 97 (D17), 18681–18695.

Gagne, W.C., Cuddihy, L.W., 1999. Vegetation.. In: Wagner, W., Herbst, D., Sohmer, S.H. (Eds.), Manual of the Flowering Plants of Hawai'i, revised edition, vol. 1. University of Hawai'i Press, pp. 45–116.

Giambelluca, T.W., 1983. Water balance of the Pearl Harbor—Honolulu basin, Hawai'i, 1946–1975. Technical Report 151. Water Resources Research Center, University of Hawai'i, Honolulu, xi + 151 pp.

Giambelluca, T.W., 1986. Land use effects on the water balance of a tropical island. National Geographic Research 2, 125–151.

Giambelluca, T.W., Nullet, M.A., Schroeder, T.A., 1986. Rainfall Atlas of Hawai'i. State of Hawai'i, Department of Land and Natural Resources, Division of Water and Land Development, Honolulu.

Giambelluca, T.W., Ridgley, M.A., Nullet, M.A., 1996. Water balance, climate change, and land-use planning in the Pearl Harbor Basin, Hawai'i. International Journal of Water Resources Development 12, 515–530.

Goulden, M.L., Munger, J.W., Fan, S.-M., Daube, B.C., Wofsy, S.C., 1996. Measurements of carbon sequestration by long-term eddy covariance: methods and a critical evaluation of accuracy. Global Change Biology 2, 160–182.

Hafkenscheid, R.L.L.J., Bruijnzeel, L.A., de Jeu, R.A.M., Bink, N.J., 2002. Water budgets of two upper montane rain forests of contrasting stature in the Blue mountains, Jamaica. In: Gladwell, J.S. (Ed.), Proceedings of the Second International Colloquium on Hydrology and Water Management, CATHALAC, Panamá City, Panamá, pp. 399–424.

Halldin, S., Lindroth, A., 1992. Errors in net radiometry: comparison and evaluation of six radiometer designs. Journal of Atmospheric and Oceanic Technology 9, 762–783.

Harrington, R.A., Fownes, J.H., Vitousek, P.M., 2001. Production and resource use efficiencies in N- and P-limited tropical forests: a comparison of responses to long-term fertilization. Ecosystems 4, 646–657.

Hodges, G.B., Smith, E.A., 1997. Intercalibration, objective analysis, intercomparison and synthesis of BOREAS surface net radiation measurements. Journal of Geophysical Research 102 (D24), 28885–28900.

Högström, U., Bergström, H., Smedman, A.-S., 1989. Turbulent fluxes above a pine forest. I. Fluxes and gradients. Boundary–Layer Meteorology 49, 197–217.

Huntingford, C., Blyth, E.M., Wood, N., Hewer, F.E., Grant, A., 1998. The effect of orography on evaporation. Boundary–Layer Meteorology 86, 487–504.

Hutley, L.B., Doley, D., Yates, D., Boonsaner, A., 1997. Water balance of an Australian subtropical rainforest at altitude: the ecological and physiological significance of intercepted cloud and fog. Australian Journal of Botany 45, 311–329.

Jackson, L.B., 1996. Digital Filters and Signal Processing: With MATLAB Exercises. Kluwer Academic Publishers, Dordrecht, The Netherlands.

Jetten, V.G., 1994. Modelling the Effects of Logging on the Water Balance of a Tropical Rain Forest: A Study of Guyana. Tropenbos Series Number 6, The Tropenbos Foundation, Wageningen, The Netherlands, 196 pp.

Jipp, P.H., Nepstad, D.C., Cassel, D.K., Reis De Carvalho, C., 1998. Deep soil moisture storage and transpiration in forests and pastures of seasonally-dry Amazonia. Climatic Change 39, 395–412.

Kaiser, J.F., 1966. Digital filters. In: Kuo, F.F., Kaiser, J.F. (Eds.), System Analysis by Digital Computer. Wiley, New York (Chapter 7).

Kumagai, T., Saitoh, T.M., Sato, Y., Takahashi, H., Manfroi, O.J., Morooka, T., Kuraji, K., Suzuki, M., Yasunari, T., Komatsu, H., 2005. Annual water balance and seasonality of evapotranspiration in a Bornean tropical rainforest. Agricultural and Forest Meteorology 128, 81–92.

Lawton, R.O., Nair, U.S., Pielke Sr., R.A., Welch, R.M., 2001. Climatic impact of tropical lowland deforestation on nearby montane cloud forests. Science 294, 584–587.

LI-COR Inc., 2004. LI-7500 open path CO_2/H_2O analyzer instruction manual. LI-COR Inc., Lincoln, NE, USA. Available online: ftp://ftp.licor.com/perm/env/LI-7500/Manual/LI-7500Manual_V4.pdf.

Malhi, Y., Pegoraro, E., Nobre, A.D., Pereira, M.G.P., Grace, J., Culf, A.D., Clement, R., 2002. The water and energy dynamics of a central Amazonian rain forest. Journal of Geophysical Research-Atmospheres 107 (D20), 8061, doi:10.1029/2001JD000623.

Massman, W.J., Finnigan, J., Billesbach, D., 2003. Summary and synthesis of recommendations of the AmeriFlux Workshop on Standardization of Flux Analysis and Diagnostics. Workshop held at Corvallis, OR, USA, August, 2002. Available online: http://cdiac.esd.ornl.gov/programs/ameriflux/workshops/Corvalis_August2002/workshop2_summary.doc.

Meesters, A.G., Vugts, H.F., 1996. Calculation of heat storage in stems. Agricultural and Forest Meteorology 78, 181–202.

Merlin, M.D., Juvik, J.O., 1993. Montane cloud forests in the tropical Pacific: some aspects of their floristics, biogeography, ecology, and conservation. In: Hamilton, L.S., Juvik, J.O., Scatena, F.N. (Eds.), Tropical Montane Cloud Forests, Proceedings of an international Symposium, San Juan, PR, May–June, 1993.

Miller, S.D., Goulden, M.L., Menton, M.C., da Rocha, H.R., de Freitas, H.C., e Silva Figuera, A.M., 2004. Biometric and micrometeorological measurements of tropical forest carbon balance. Ecological Applications 14, S114–S126.

Mink, J.F., 1962. Rainfall and runoff in the leeward Koolau mountains, Oahu, Hawaii. Pacific Science 16, 147–159.
Monteith, J.L., 1973. Principles of Environmental Physics. Elsevier, New York.
Moore, C.J., Fisch, G., 1986. Estimating heat storage in Amazonian tropical forest. Agricultural and Forest Meteorology 38, 147–168.
Mudd, R.G., 2004. Significance of the epiphyte layer to stem water storage in native and invaded tropical montane cloud forests in Hawai'i. Senior Thesis. Global Environmental Science, University of Hawai'i at Mānoa.
Noormets, A., Chen, J., Crow, T.R., 2007. Age-dependent changes in ecosystem carbon fluxes in managed forests in northern Wisconsin, USA. Ecosystems 10, 187–203.
Oki, D.S., 2002. Reassessment of ground-water recharge and simulated ground-water availability for the Hawii area of North Kohala, Hawai'i. Water-Resources Investigations Report 02-4006. U.S. Geological Survey, Honolulu, vi + 62 pp.
Philip, J.R., 1961. The theory of heat flux meters. Journal of Geophysical Research 66, 571–579.
Pounds, J.A., Fogden, M.P.L., Campbell, J.H., 1999. Biological response to climate change on a tropical mountain. Nature 398, 611–615.
Raich, J.W., Riley, R.H., Vitousek, P.M., 1994. Use of root-ingrowth cores to assess nutrient limitations in forest ecosystems. Canadian Journal of Forest Research 24, 2135–2138.
Raich, J.W., Russell, A.E., Vitousek, P.M., 1997. Primary productivity and ecosystem development along an elevational gradient on Mauna Loa, Hawaii. Ecology 78, 707–721.
Saleska, S.R., et al., 2003. Carbon in Amazon forests: unexpected seasonal fluxes and disturbance-induced losses. Science 302, 1554–1557.
Sandström, F., Petersson, H., Kruys, N., Ståhl, G., 2007. Biomass conversion factors (density and carbon concentration) by decay classes for dead wood of *Pinus sylvestris*, *Picea abies* and *Betula* spp. in boreal forests of Sweden. Forest Ecology and Management 243, 19–27.
Scatena, F.N., 1990. Watershed scale rainfall interception on two forested watersheds in the Luquillo mountains of Puerto Rico. Journal of Hydrology 113, 89–102.
Schellekens, J., Bruijnzeel, L.A., Scatena, F.N., Bink, N.J., Holwerda, F., 2000. Evaporation from a tropical rain forests, Luquillo Experimental Forest, eastern Puerto Rico. Water Resources Research 36, 2183–2196.
Schuepp, P.H., Leclerc, M.Y., MacPherson, J.I., Desjardins, R.L., 1990. Footprint prediction of scalar fluxes from analytical solutions of the diffusion equation. Boundary–Layer Meteorology 50, 355–373.
Shade, P.J., 1995a. Water budget for the Island of Kauai, Hawaii. Water Resources Investigations Report 95-4128. U.S. Geological Survey, Honolulu, iv + 25 pp.
Shade, P.J., 1995b. Water budget for the Kohala area, Island of Hawaii. Water Resources Investigations Report 95-4114. U.S. Geological Survey, Honolulu, iv + 19 pp.
Shade, P.J., 1997. Water budget for the Island of Molokai, Hawaii. Water Resources Investigations Report 97-4155. U.S. Geological Survey, Honolulu, iv + 20 pp.
Shuttleworth, W.J., 1988. Evaporation from Amazonian rainforest. Proceedings of the Royal Society of London B 233, 321–346.
Shuttleworth, W.J., 1989. Micrometeorology of temperate and tropical forest. Philosophical Transactions of the Royal Society, Series B 324, 299–334.
Silberstein, R., Held, A., Hatton, T., Viney, N., Sivapalan, M., 2001. Energy balance of a natural jarrah (*Eucalyptus marginata*) forest in Western Australia: measurements during the spring and summer. Agricultural and Forest Meteorology 109, 79–104.
Still, C.J., Foster, P.N., Schneider, S.H., 1999. Simulating the effects of climate change on tropical montane cloud forests. Nature 398, 608–610.
Stone, C.P., Pratt, L.W., 1994. Hawai'i's Plants and Animals: Biological Sketches of Hawai'i Volcanoes National Park. Hawaii Natural History Association, National Park Service, and University of Hawaii Cooperative National Park Resources Study Unit, 399 pp.
Takasaki, K.J., Hirashima, G.T., Lubke, E.R., 1969. Water resources of windward Oahu. Geological Survey Water-Supply Paper 1894. U.S. Department of the Interior, Washington, DC, 119 pp.
Tani, M., Abdul Rahim, N., Yasuda, Y., Noguchi, S., Siti Aisah, S., Mohd Md, S., Takanashi, S., 2003. Long-term estimation of evapotranspiration from a tropical rain forest in Peninsular Malaysia. In: Franks, S., Bloeschl, G., Kumagai, M., Musiake, K., Rosbjerg, D. (Eds.), Water Resources Systems—Water Availability and Global Change. IAHS Publ. No. 280, IAHS Press, Wallingford, pp. 267–274.
Tanner, C.B., Thurtell, G.W., 1969. Anemoclinometer Measurements of Reynolds Stress and Heat Transport in the Atmospheric Surface Layer. University of Wisconsin Tech. Rep. ECOM-66-G22-F, 82 pp.
ter Steege, H., Boot, R., Brouwer, L., Hammond, D., van der Hout, P., Jetten, V.G., Khan, Z., Polak, A.M., Raaimakers, D., Zagt, R., 1995. Basic and applied research for sound rain forest management in Guyana. Ecological Applications 5, 904–910.
Twine, T.E., Kustas, W.P., Norman, J.M., Cook, D.R., Houser, P.R., Meyers, T.P., Prueger, J.H., Starkds, P.J., Wesely, M.L., 2000. Correcting eddy-covariance flux underestimates over a grassland. Agricultural and Forest Meteorology 103, 279–300.
Van der Molen, 2002. Meteorological impacts of land use change in the maritime tropics. PhD dissertation, Vrije Universiteit, Amsterdam, The Netherlands, 262 pp.
von Randow, C., Manzi, A.O., Kruijt, B., de Oliveira, P.J., Zanchi, F.B., Silva, R.L., Hodnett, M.G., Gash, J.H.C., Elbers, J.A., Waterloo, M.J., Cardoso, F.L., Kabat, P., 2004. Comparative measurements and seasonal variations in energy and carbon exchange over forest and pasture in South West Amazonia. Theoretical and Applied Climatology 78 5–26, 2004.
Waterloo, M.J., Bruijnzeel, L.A., Vugts, H.F., Rawaqa, T.T., 1999. Evaporation from *Pinus caribaea* plantations on former grassland soil under maritime tropical conditions. Water Resources Research 35, 2133–2144.
Webb, E.K., Pearman, G.I., Leuning, R., 1980. Correction of flux measurements for density effects due to heat and water vapor transfer. Quarterly Journal of the Royal Meteorological Society 106, 67–90.
Wilczak, J.M., Oncley, S.P., Stage, S.A., 2001. Sonic anemometer tilt correction algorithms. Boundary–Layer Meteorology 99, 127–150.
Wilson, K.B., Baldocchi, D.D., 2000. Seasonal and interannual variability of energy fluxes over a broadleaved temperate deciduous forest in North America. Agricultural and Forest Meteorology 100, 1–18.
Wilson, K., Goldstein, A., Falge, E., Aubinet, M., Baldocchi, D., Berbigier, P., Bernhofer, C., Ceulemans, R., Dolman, H., Field, C., Ibrom, A.G.A., Law, B.E., Kowalski, A., Meyers, T., Moncrieff, J., Monson, R., Oechel, W., Tenhunen, J., Valentini, R., Verma, S., 2002. Energy balance closure at FLUXNET sites. Agricultural and Forest Meteorology 113, 223–243.
Wolfe, E.W., Morris, J., 1996. Geologic map of the Island of Hawai'i. USGS IMAP Series No. 2524-A. U.S. Geological Survey.